Rapid Communications

Tides in merging neutron stars: Consistency of the GW170817 event with experimental data on finite nuclei

Tuhin Malik,[1,*] B. K. Agrawal,[2,3] J. N. De,[2] S. K. Samaddar,[2] C. Providência,[4] C. Mondal,[5] and T. K. Jha[1]

[1]*Department of Physics, BITS-Pilani, K.K. Birla Goa Campus, Goa 403726, India*

[2]*Saha Institute of Nuclear Physics, 1/AF Bidhannagar, Kolkata 700064, India*

[3]*Homi Bhabha National Institute, Anushakti Nagar, Mumbai 400094, India*

[4]*CFisUC, Department of Physics, University of Coimbra, 3004-516 Coimbra, Portugal*

[5]*Departament de Física Quàntica i Astrofísica and Institut de Ciències del Cosmos (ICCUB), Facultat de Física, Universitat de Barcelona, Martí i Franquès 1, E-08028 Barcelona, Spain*

(Received 28 January 2019; revised manuscript received 25 March 2019; published 20 May 2019)

The agreement of the nuclear equation of state (EOS) deduced from the GW170817-based tidal deformability with the one obtained from empirical data on microscopic nuclei is examined. It is found that suitably chosen experimental data on isoscalar and isovector modes of nuclear excitations together with the observed maximum neutron star mass constrain the EOS which displays a very good congruence with the GW170817 inspired one. The giant resonances in nuclei are found to be instrumental in limiting the tidal deformability parameter and the radius of a neutron star in somewhat narrower bounds. At the 1σ level, the values of the canonical tidal deformability $\Lambda_{1.4}$ and the neutron star radius $R_{1.4}$ come out to be 267 ± 144 and 11.6 ± 1.0 km, respectively.

DOI: 10.1103/PhysRevC.99.052801

Introduction. After the detection of gravitational waves from the GW170817 binary neutron star merger event [1], the rich connection between the very large and the very small nuclear objects has developed more intensely. During the last stages of the inspiral motion of the coalescing neutron stars (NSs), the strong gravity of each of them induces a tidal deformation in the companion star. Decoding the gravitational wave phase evolution caused by that deformation [2] allows the determination of the dimensionless tidal deformability parameter Λ [3–5]. It is a measure of the response to the gravitational pull on the neutron star surface correlating with pressure gradients inside the NS and, therefore, it has been proposed as an effective probe of the equation of state (EOS) of nuclear matter relevant for neutron stars [6,7]. A comparatively large value of Λ, for example, points to a neutron star of large radius [8–10]. This translates into a stiffer nuclear matter EOS and, hence, a comparatively larger neutron skin of a heavy nucleus on the terrestrial plane [11]. Early analysis of the GW170817 event [1] puts an upper limit to the binary tidal deformability $\tilde{\Lambda}$ at $\approx$800 for the component neutron stars with masses in the range $\approx 1.17 M_\odot$–$1.6 M_\odot$ involved in the merger event under the low-spin prior scenario. $\tilde{\Lambda}$ is defined as

$$\tilde{\Lambda} = \frac{16}{13}\frac{(12q+1)\Lambda_1 + (12+q)q^4\Lambda_2}{(1+q)^5}, \qquad (1)$$

where $\Lambda_{1,2}$ are the tidal deformabilities of the neutron stars of masses M_1 and M_2 and $q = M_2/M_1 \leqslant 1$ is the binary's mass ratio. The masses of the binary components are constrained by the chirp mass $\mathcal{M} = (M_1 M_2)^{3/5}/(M_1+M_2)^{1/5} = 1.188 M_\odot$ for the GW170817 event, where $M_\odot$ is the solar mass. When $q = 1$, $\tilde{\Lambda}$ reduces to Λ and is calculated from $\Lambda = \frac{2}{3} k_2 [\frac{c^2 R}{GM}]^5$, where k_2 is the second Love number [1], R being the radius of the neutron star. After the initial proposition, the value of $\tilde{\Lambda}$ has gone through several revisions [9,12,13]. Reference [9] reported $\tilde{\Lambda} = 222^{+420}_{-138}$ for a uniform component-mass prior at the 90% credible level; with a few plausible assumptions, a restrictive constraint is now set for a canonical Λ ($=\Lambda_{1.4}$, for a neutron star of mass $1.4 M_\odot$) at 190^{+390}_{-120} [13] and the radii of both the lighter and the heavier neutron stars in the merger event at $R_{1,2} = 11.9 \pm 1.4$ km. From the spectral parametrization of the defining function $p(\rho)$ (p = pressure) to fit the observational template, the pressure inside the NS at supranormal densities is also predicted. Complementing the electromagnetic probes that determine the maximum mass of neutron stars ($2.01^{+0.04}_{-0.04} \leqslant M_{\rm NS}^{\rm max}/M_\odot \leqslant 2.16^{+0.17}_{-0.15}$) [14–16], GW-based probes of the neutron star structure thus set the stage for exploring the nuclear matter EOS at large densities.

First-principle calculations of the nuclear matter EOS at subsaturation densities in chiral effective field theory (CEFT) [17] and at very high densities in perturbative QCD [18,19] are robust. The problem of generating the most generic family of NS-matter EOSs at intermediate densities that interpolates between these reliable theoretical estimates consistent with the observational constraints on $M_{\rm NS}^{\rm max}$ and the tidal deformability has been recently addressed [8]. A significant constraint on the nuclear matter EOS is found from the inspection that the low-density EOS must be stiff enough to support a NS of mass $\approx 2 M_\odot$ but soft enough so

*tuhin.malik@gmail.com

that $\tilde{\Lambda} < 800$ [12]. Revisiting this problem with a huge number of parametrically constructed plausible different EOSs connecting the low- and the high-density ends, Most *et al.* [20] found that, for a purely hadronic star, the tidal deformability is constrained at $\Lambda_{1.4} > 375$ at 2σ confidence level. A nonparametric method for inferring the universal neutron star matter EOS from GW observations iwas also reported recently [21] with the canonical deformability $\Lambda_{1.4} = 160^{+448}_{-133}$ at 90% confidence level. A lower bound on the tidal deformability $\approx$400 is also set from the analysis of the UV-optical-infrared counterpart of GW170817 complemented with numerical relativity results [22]. Similar analysis, but with a larger number of models, pushes the lower bound to $\approx$200 [23].

Through a combination of laboratory data on light nuclei and sophisticated microscopic modeling of the subsaturation EOS from CEFT [24–27], attempts have been made to arrive at values of the tidal deformability. Using a relativistic mean field (RMF) inspired family of EOS models calibrated to provide a good description of a set of selective properties of finite nuclei, the impact of the tidal deformability on the neutron skin of ^{208}Pb and on the NS mass and radius has also been addressed [11]. The varying outcomes point to the fact that the connection of the tidal deformability to the laboratory data is not yet fully transparent and that more stringent constraints on the isovector sector of the effective interaction are needed. From new-found strong correlations of $\Lambda_{1.4}$ and $R_{1.4}$ with a set of selective linear combinations of isoscalar and isovector properties of nuclear matter, it is realized that such constraints may be provided by the isovector giant resonances in conjunction with the isoscalar resonances in finite nuclei.

To have a better understanding of these particularities, in this communication, we perform an analysis of the suitability of some often-used Skyrme models to explain isoscalar and isovector giant resonance data and examine their predictions for $\Lambda_{1.4}$. Simultaneously, attention is given to the analysis of the astrophysical constraint on the neutron star maximum mass $M_{\rm NS}^{\rm max}$ [14,15]; this encodes pressure gradient information from mapping the varying neutron-proton asymmetry over a large density range. Later, by fitting a broader based set of isoscalar and isovector data along with the observed NS mass constraint, we propose a new EOS with the uncertainties estimated within the covariance analysis and check its compatibility with the GW data. The calculation is model dependent in the sense that the EOS is taken to be a smooth function of density and avoids possibilities of phase transitions to exotic forms of matter when more drastic changes in the density behavior of the EOS are considered.

Motivation from existing trends. We resort to the Skyrme framework for this study. For the suitability analysis of the Skyrme EDFs, we choose among them 28 EDFs that are more representative. They include the set of 13 "best" EDFs (CSkP set) used in Ref. [28]. These are: KDE0v1, LNS, NRAPR, Ska25s20, Ska35s20, SKRA, SkT1, SkT2, SkT3, SQMC700, Sv-sym32, Sly4, and SkM*. Another set of 13 Skyme EDFs used in Ref. [29] are also taken to examine the correlation of the neutron star radius with some key parameters of symmetric and asymmetric nuclear matter. They are Ska, Skb, SkI2, SkI3, SkI5, SkI6, Sly2, Sly230a, Sly9, SkMP, SkOP, SK255, and SK272. To this list of 26, two recent EDFs, Skχm* [30] and KDE0-J34 [31] are further included; they are compliant with the measured dipole polarizability of few nuclei. The Skχm* EDF, in addition, reproduces the theoretical predictions on properties of asymmetric nuclear matter from CEFT [32,33]. All these EDFs provide a satisfactory reproduction of the binding energies of finite nuclei and their charge radii, and obey reasonable constraints on the properties of symmetric nuclear matter such as the energy per nucleon ($e_0 = -15.8 \pm 0.5$ MeV), the saturation density ($\rho_0 = 0.16 \pm 0.01$ fm^{-3}), the isoscalar nucleon effective mass ($\frac{m_0^*}{m} = 0.6$–1.0) and the isoscalar nuclear incompressibility($K_0 = 240 \pm 30$ MeV).

The 28 EDFs mentioned above were constructed with emphasis on different biases for the selection of data on finite nuclei and nuclear matter properties. We would like to have a closer look into these EDFs by analyzing their ability to explain a few further significant data related to isoscalar and isovector properties of finite nuclei and draw inferences on the consistency of the EDFs in explaining observables concerning neutron star masses and their tidal deformability. The experimental data of particular interest for finite nuclei are the centroid energy $E^{\rm c}_{\rm GMR}$ of the isoscalar giant monopole resonance (ISGMR), the peak energy $E^{\rm p}_{\rm GDR}$ of the isovector giant dipole resonance (IVGDR), and the dipole polarizability α_D, all for the heavy nucleus ^{208}Pb. The dipole polarizability α_D and the GDR peak energies are measures of the isovector parameter Θ_v, which defines the isovector effective nucleon mass $m^*_{v,0}$ [34] in the Skyrme methodology. In conjunction with the isoscalar effective mass m_0^*, this determines the isovector splitting of the nucleon effective mass [$\Delta m_0^* \equiv (m_n^* - m_p^*)/m$], which is directly related to the isovector properties of the nuclear interaction. Concerning the astrophysical context, the data include the observed lower limit of the maximum mass $M_{\rm NS}^{\rm max}$ of the neutron star [14,15], ($M_{\rm NS}^{\rm max} = 2.01 \pm 0.04 M_\odot$).

The constraints provided by these empirical data allow us to choose the most plausible EDFs considering the neutron star maximum mass and its radius, and the tidal deformability parameter along with other properties of nuclear matter like m_0^* or Δm_0^*. For the selected 28 EDFs, we find the effective mass $\frac{m_0^*}{m}$ lying between $\approx$0.6 and 1.0 with Δm_0^* distributed nearly evenly with positive and negative signs. This is shown as (+) and (−) signs for Δm_0^* superimposed on the symbols in Fig. 1(a) where the calculated values of $M_{\rm NS}^{\rm max}$ are given as a function of the tidal deformability parameter $\Lambda_{1.4}$ for the given EDFs. To focus on the role of m_0^* in determining the ISGMR energy and the maximum mass of the neutron star, $\frac{m_0^*}{m}$ of the EDFs are sorted in three groups: $0.60 \leqslant \frac{m_0^*}{m} < 0.65$ (red solid circle), $0.65 \leqslant \frac{m_0^*}{m} < 0.75$ (blue solid square), and $0.75 \leqslant \frac{m_0^*}{m} \leqslant 1.0$ (green solid pentagon). The red dashed horizontal lines in all the four panels in Fig. 1 show the lower bound of the observed maximum value of the NS mass ($=1.97 M_\odot$) that an acceptable EDF must support. To calculate the neutron star properties, the EOS for its crust is taken from the Baym, Pethick, and Sutherland model [35] in the density range $\rho \approx 4.8 \times 10^{-9}$ to 2.6×10^{-4} fm^{-3}. The structure of the core is calculated from the EDFs with the assumption

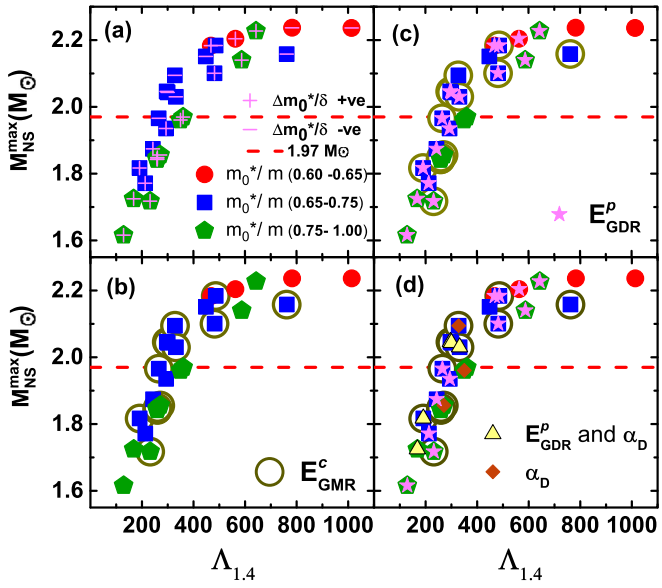

FIG. 1. The maximum neutron star mass $M_{\rm NS}^{\rm max}$ versus the tidal deformability parameter $\Lambda_{1.4}$ obtained from the 28 selected EDFs. The red dashed lines refer to $1.97M_\odot$, the observed lower bound for $M_{\rm NS}^{\rm max}$. For more details, see text.

of a charge neutral uniform plasma of neutrons, protons, electrons, and muons in β equilibrium. The EOS for the region between the inner edge of the outer crust and the beginning of the outer core defined by the crust-core transition density is appropriately interpolated using a polytropic form [36]. This method may introduce uncertainties in the determination of the radius of low and intermediate NS masses [37–39]. We have estimated an average uncertainty of ≈2% on $\Lambda_{1.4}$ by comparing the present results with the ones obtained from unified EOSs. Figure 1(a) shows that the constraint on the NS maximum mass alone filters out some EDFs. A good fraction of the EDFs with effective masses above 0.75 m fail to achieve the lower bound on $M_{\rm NS}^{\rm max}$.

EDFs that fulfill the constraint imposed by the ISGMR centroid energy in ^{208}Pb (14.17 ± 0.28 MeV) are represented by additional open circles in Fig. 1(b). The EDFs with effective masses in the lower end of the spectrum (red solid circles, $\frac{m_0^*}{m} < 0.65$) are seen to be excluded from consideration; lower effective masses tend to yield higher values of ISGMR energies than desired. The further constraint of satisfying the IVGDR peak energy (13.43 MeV; in Ref. [40], a large width of 4.07 MeV is ascribed to it; we take a conservative estimate of 2 MeV for the width) for ^{208}Pb (marked with further magenta-colored star) eliminates a few more EDFs as shown in Fig. 1(c) and, as is also seen there, it forces the focus on effective mass values in the middle range (0.65–0.75) m. On top of these, imposition of the next constraint concerning the dipole polarizability α_D for ^{208}Pb (19.6 ± 0.6 fm^3) leaves open the question of the suitability of most of the EDFs, as is seen from the inspection of Fig. 1(d). EDFs satisfying the constraint on α_D are marked by orange diamonds, those satisfying criteria concerning both the IVGDR peak energy and α_D are marked by yellow triangles (see Table I of the Supplemental Material [41] for details on 28 EDFs). Figure 1(d) shows that among the 28 selected EDFs, only three satisfy all the constraints considered. They are the interactions Sly2, Sly4, and KDE0-J34. For these three EDFs, the effective mass is ≈0.7m, and the isovector mass splitting Δm_0^* is negative. It is of interest to note that the constraints on the maximum NS mass and the ISGMR datum in ^{208}Pb cannot delineate the sign of the values of Δm_0^*, positive or negative; the extra constraint on the peak energy of IVGDR in ^{208}Pb is in favor of a negative Δm_0^*, the final constraint on the dipole polarizability settles this issue. The value of the nucleon effective mass (0.7m) is in very good agreement with that obtained from the optical model analysis of nucleon-nucleus scattering [42], but the negative value of the isospin-split effective mass, at variance with most theoretical predictions [34,42–49], needs possibly a more critical examination. Presently we do not discuss this matter except mentioning that a recent EDF [50] based on the Gibbs-Duhem relation and specifically designed to fit a wide variety of pseudodata corresponding to infinite nuclear matter and the experimental energy weighted sum rule for a few nuclei yields a value for the nucleon effective mass that is very close ($\frac{m_0^*}{m} = 0.68$) to what we find from this analysis and also gives a negative value for $\Delta m_0^*(= -0.2\delta)$. Here, δ is the isospin asymmetry of nuclear matter defined as $\delta = (\rho_n - \rho_p)/\rho$, ρ_n and ρ_p being the neutron and proton densities, respectively.

The role of the empirical data in sensitively constraining the tidal deformability parameter Λ should now be stressed. One sees from Fig. 1 that from the total 28 EDFs chosen, $\Lambda_{1.4}$ stretches out from 100 to 1000, the NS mass constraint shrinks the bandwidth to ≈270–1000, the ISGMR datum shrinks it to ≈270–760, the IVGDR peak energy squeezes it further to ≈270–590, and $\Lambda_{1.4}$ settles it at ≈290–330 when filtered through the choices of all the data considered; it lies midway of the observed bandwidth for $\Lambda_{1.4}$ deduced from the GW170817 event [13]. This survey suggests that there are models that can endure the constraint on the observed $M_{\rm NS}^{\rm max}$, but many of them would not fit the experimental data on the properties of the ISGMR and IVGDR simultaneously due to the weak correlations among them as discussed later. We would like to emphasize that the conclusion drawn from Fig. 1 is only indicative of the value of the tidal deformability and serves as the motivation for the quantitative investigation that follows.

Constraining tidal deformability from measured properties of finite nuclei. To reassess the bounds on the tidal deformability more accurately, a new Skyrme EDF calibrated with a wider fit data base is proposed. The constraints include the observed maximum NS mass $M_{\rm NS}^{\rm max}$, the binding energies of spherical magic nuclei, their charge radii, the ISGMR energy of ^{208}Pb, and its dipole polarizability. In addition, the ISGMR energies of ^{90}Zr and ^{120}Sn and the dipole polarizability α_D of ^{48}Ca, ^{68}Ni, and ^{120}Sn are included in the fitting protocol.

It is observed that for the models employed in Fig. 1, $E^c_{\rm GMR}$, α_D, and $M_{\rm NS}^{\rm max}$ are weakly correlated among themselves (Pearson correlation coefficients r are ≈ 0.5). Simultaneously constraining these quantities may impose strong restrictions on the model parameters. The IVGDR peak energies are left out of the fitting protocol deliberately. Calculations with the selected EDFs reveal the existence of an anticorrelation of

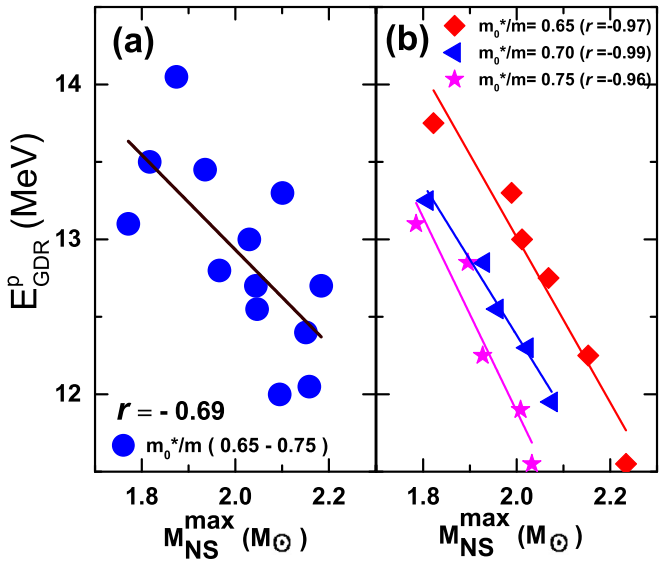

FIG. 2. Correlation of E^{p}_{GDR} and M^{max}_{NS} obtained using (a) the set of selected models as in Fig. 1 with effective mass m_0^*/m in the range 0.65–0.75 and (b) a set of systematically varied models with chosen fixed effective masses in the present work.

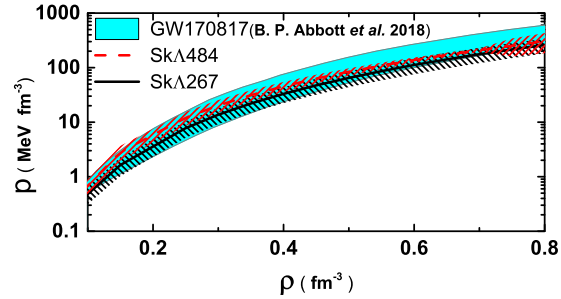

FIG. 3. Pressure of β-equilibrated neutron star matter displayed as a function of density. The shaded region represents the constraints from the GW170817 event (B.P. Abbott *et. al* 2018: [13]).

E^{p}_{GDR} for ^{208}Pb with M^{max}_{NS} when the EDFs are sorted in groups within narrow windows in m_0^*/m. For illustration, this anticorrelation is displayed in Fig. 2(a) for effective masses in the range $0.65 \leqslant m_0^*/m < 0.75$ with the selected EDFs. The correlation coefficient is $r = -0.69$. However, we see that the aforesaid correlation shoots up to nearly unity when calculated with the systematically varied models obtained with fixed values of m_0^*/m as displayed in Fig. 2(b). For given values of M^{max}_{NS} and m_0^*/m, E^{p}_{GDR} is the outcome of the calculation keeping all other data in the fitting protocol unchanged.

The optimized χ^2 function from the fit to all the input data (M^{max}_{NS} and measured properties of finite nuclei as mentioned) yields the EDF parameters. They are listed in Table I along with their errors obtained within the covariance method [30,51,52]. Some selected properties of nuclear matter and neutron stars are also presented in the table. Since the central value of $\Lambda_{1.4}$ comes out to be 267, we hereafter name this EDF SkΛ267. The nuclear matter constants obtained for SkΛ267 are in excellent agreement with their fiducial values. The lower bound on M^{max}_{NS} is comfortably obeyed; the tidal deformability parameter $\Lambda_{1.4}$ and the NS radius $R_{1.4}$ are also found to be in very good agreement with those reported in Ref. [13], the errors are more contained though. The value of the neutron-skin Δr_{np} for ^{208}Pb is 0.15 ± 0.05 fm.

Since the experimental value of tidal deformability is not yet settled, tolerance of the fit of the calculated observables with the data is further tested by arbitrarily constraining $\Lambda_{1.4}$ to different values. As a demonstrative example we use an extra constraint in our fit $\Lambda_{1.4} = 500 \pm 100$. The outcome is model SkΛ484 with $\Lambda_{1.4} = 484$ (see Table IV of the Supplemental Material [41] for the parameters). The model SkΛ267 is found to be more compatible with the measured properties of finite nuclei. A comparison of different observables related to nuclear matter and NS properties calculated with SkΛ267 and SkΛ484 is given in Tables III and IV of the Supplemental Material [41]. One may note the closeness of the nuclear matter observables obtained from SkΛ267 and those from the interaction SLy4 [53]. In SLy4, instead of the IVGDR as fit data as used in this paper, the isotopic properties of forces beyond the β stability line were dictated by having a good reproduction of neutron-matter EOS obtained variationally by Wiringa *et al.* [54,55].

The prediction of the EOSs SkΛ267 and SkΛ484 for the pressure of the neutron star matter as a function of density is displayed in Fig. 3 and compared with that deduced from the GW170817 event [13]. As expected, SkΛ267 is somewhat softer than SkΛ484. Overall, the agreement between theory and experiment is very good; the delineation among the two theoretical EOSs is, however, done through the microscopic lens of the measured properties of finite nuclei as already stated. Both EDFs maintain causality in the density range encountered in the interior of the neutron stars; they become acausal beyond $\rho \approx 8\rho_0$ which is slightly higher than the central density $\approx 7.0\rho_0$ for the maximum mass.

TABLE I. Parameters for the model SkΛ267 and the resulting nuclear matter and neutron star properties along with their errors in parentheses. J_0 is the symmetry energy coefficient, L_0 is related to its density derivative [50].

t_0 (MeV fm^3)	t_1 (MeV fm^5)	t_2 (MeV fm^5)	t_3 (MeV fm$^{3+3\alpha}$)	x_0	x_1	x_2	x_3	α	W_0(MeV fm^5)
−2481.08	482.51	−516.17	13778.74	0.93	−0.53	−0.97	1.54	0.167	121.38
(89.05)	(50.41)	(407.22)	(123.72)	(0.28)	(0.89)	(0.20)	(0.58)	(0.018)	(9.35)
e_0 (MeV)	ρ_0 (fm^{-3})	K_0 (MeV)	m_0^*/m	J_0 (MeV)	L_0 (MeV)	$\Delta m_0^*/\delta$	$\Lambda_{1.4}$	$R_{1.4}$ (km)	M^{max}_{NS} ($M_\odot$)
16.04	0.162	230.2	0.70	31.4	41.1	−0.25	267	11.6	2.04
(0.20)	(0.002)	(6.4)	(0.05)	(3.1)	(18.2)	(0.35)	(144)	(1.0)	(0.15)

Remarks. GW-based measurements of the macroscopic properties of neutron stars offer a very promising means of looking deeper into the nuclear microphysics governing the internal structure of the neutron stars and of obtaining sound informative constraints on the nuclear EOS at subnormal and supranormal densities. We have explored in this communication how the low-density laboratory-data-inspired nuclear matter EOS connects with that obtained from GW-based data. We show that the pressure-density variation deduced from GW analysis is in very good agreement with a parametric form of the EOS designed to comply with properly chosen nuclear observables sensitive to the isoscalar and isovector parts of the nuclear interaction together with the NS mass constraint. The tidal deformability parameter is now constrained at $\approx 267 \pm 144$ (267 ± 236) at 1σ level (90% confidence level). We note that a recent reanalysis [56] of the GW-based data leads to a considerable stretching of the bounds on the tidal deformability although the central value ($\approx$200) maintains an extremely good consistency with those obtained earlier or with that obtained by us. On the other hand, the EOS derived from a neural network [57] having as input observational data from several neutron stars leads to $\Lambda_{1.4} = 320 \pm 120$ which is entirely consistent with the values derived here. Constraining NS properties from low-energy nuclear physics thus seems very meaningful. All nuclear properties, both isoscalar and isovector, derived from our EOS are in very comfortable agreement with their fiducial values. The values of the incompressibility, the symmetry energy, and its density derivative indicate that the EOS is soft at densities near saturation; the conformity of the low value of the tidal deformability with the most recent estimates shows that the EOS is soft over a wider range of densities and thus leaves the question open as to how to identify a possible phase transition in the neutron star core. Future detections of binary star mergers by the LIGO-Virgo Collaboration may settle this issue.

Acknowledgments. The authors acknowledge kind assistance from Tanuja Agrawal in the preparation of the manuscript. J.N.D. acknowledges support from the Department of Science and Technology, Government of India with Grant No. EMR/2016/001512. C.P. acknowledges financial support by Fundação para a Ciência e Tecnologia (FCT) Portugal under Project No. UID/FIS/04564/2019, Project POCI-01-0145-FEDER-029912 with financial support from POCI, in its FEDER component, and by the FCT/MCTES budget through national funds (OE), and the COST action CA16214 "PHAROS". C.M. acknowledges support from Project MDM-2014-0369 of ICCUB (Unidad de Exelencia María de Maeztu) from MINECO.

[1] B. P. Abbott, R. Abbott, T. D. Abbott, F. Acernese, K. Ackley, C. Adams, T. Adams, P. Addesso, R. X. Adhikari, V. B. Adya *et al.*, Phys. Rev. Lett. **119**, 161101 (2017).
[2] E. E. Flanagan and T. Hinderer, Phys. Rev. D **77**, 021502(R) (2008).
[3] T. Hinderer, Astrophys. J. **677**, 1216 (2008).
[4] T. Hinderer, B. D. Lackey, R. N. Lang, and J. S. Read, Phys. Rev. D **81**, 123016 (2010).
[5] T. Damour, A. Nagar, and L. Villain, Phys. Rev. D **85**, 123007 (2012).
[6] K. Thorne, *Three Hundred Years of Gravitation* (Cambridge University, Cambridge, UK, 1987), p. 684.
[7] J. S. Read, C. Markakis, M. Shibata, K. Uryū, J. D. E. Creighton, and J. L. Friedman, Phys. Rev. D **79**, 124033 (2009).
[8] E. Annala, T. Gorda, A. Kurkela, and A. Vuorinen, Phys. Rev. Lett. **120**, 172703 (2018).
[9] S. De, D. Finstad, J. M. Lattimer, D. A. Brown, E. Berger, and C. M. Biwer, Phys. Rev. Lett. **121**, 091102 (2018).
[10] T. Malik, N. Alam, M. Fortin, C. Providência, B. K. Agrawal, T. K. Jha, B. Kumar, and S. K. Patra, Phys. Rev. C **98**, 035804 (2018).
[11] F. J. Fattoyev, J. Piekarewicz, and C. J. Horowitz, Phys. Rev. Lett. **120**, 172702 (2018).
[12] B. P. Abbott *et al.* (LIGO Scientific, Virgo Collaboration), Phys. Rev. X **9**, 011001 (2019).
[13] B. P. Abbott, R. Abbott, T. D. Abbott, F. Acernese, K. Ackley, C. Adams, T. Adams, P. Addesso, R. X. Adhikari, V. B. Adya *et al.*, Phys. Rev. Lett. **121**, 161101 (2018).
[14] P. Demorest, T. Pennucci, S. Ransom, M. Roberts, and J. Hessels, Nature **467**, 1081 (2010).
[15] J. Antoniadis, P. C. C. Freire, N. Wex, T. M. Tauris, R. S. Lynch, M. H. van Kerkwijk, M. Kramer, C. Bassa, V. S. Dhillon, T. Driebe *et al.*, Science **340**, 448 (2013).
[16] L. Rezzolla, E. R. Most, and L. R. Weih, Astrophys. J. Lett. **852**, L25 (2018).
[17] I. Tews, T. Krüger, K. Hebeler, and A. Schwenk, Phys. Rev. Lett. **110**, 032504 (2013).
[18] A. Kurkela, P. Romatschke, and A. Vuorinen, Phys. Rev. D **81**, 105021 (2010).
[19] E. S. Fraga, A. Kurkela, and A. Vuorinen, Eur. Phys. J. A **52**, 49 (2016).
[20] E. R. Most, L. R. Weih, L. Rezzolla, and J. Schaffner-Bielich, Phys. Rev. Lett. **120**, 261103 (2018).
[21] P. Landry and R. Essick, Phys. Rev. D **99**, 084049 (2019).
[22] D. Radice, A. Perego, F. Zappa, and S. Bernuzzi, Astrophys. J. Lett. **852**, L29 (2018).
[23] A. Bauswein, Talk delivered at International School of Nuclear Physics, 2018 (unpublished), https://crunch.ikp.physik.tu-darmstadt.de/erice/2018/sec/talks/sunday/bauswein.pdf.
[24] I. Tews, J. Margueron, and S. Reddy, Phys. Rev. C **98**, 045804 (2018).
[25] I. Tews, J. Margueron, and S. Reddy, arXiv:1901.09874.
[26] Y. Lim and J. W. Holt, Phys. Rev. Lett. **121**, 062701 (2018).
[27] Y. Lim and J. W. Holt, arXiv:1902.05502.
[28] B. A. Brown, Phys. Rev. Lett. **111**, 232502 (2013).
[29] N. Alam, B. K. Agrawal, M. Fortin, H. Pais, C. Providência, A. R. Raduta, and A. Sulaksono, Phys. Rev. C **94**, 052801(R) (2016).
[30] Z. Zhang, Y. Lim, J. W. Holt, and C. M. Ko, Phys. Lett. B **777**, 73 (2018).
[31] X. Roca-Maza, X. Viñas, M. Centelles, B. K. Agrawal, G. Colò, N. Paar, J. Piekarewicz, and D. Vretenar, Phys. Rev. C **92**, 064304 (2015).
[32] C. Wellenhofer, J. W. Holt, and N. Kaiser, Phys. Rev. C **92**, 015801 (2015).

[33] C. Wellenhofer, J. W. Holt, and N. Kaiser, Phys. Rev. C **93**, 055802 (2016).
[34] Z. Zhang and L.-W. Chen, Phys. Rev. C **93**, 034335 (2016).
[35] G. Baym, C. Pethick, and P. Sutherland, Astrophys. J. **170**, 299 (1971).
[36] J. Carriere, C. Horowitz, and J. Piekarewicz, Astrophys. J. **593**, 463 (2003).
[37] J. Piekarewicz, F. J. Fattoyev, and C. J. Horowitz, Phys. Rev. C **90**, 015803 (2014).
[38] M. Fortin, C. Providencia, A. R. Raduta, F. Gulminelli, J. L. Zdunik, P. Haensel, and M. Bejger, Phys. Rev. C **94**, 035804 (2016).
[39] H. Pais and C. Providência, Phys. Rev. C **94**, 015808 (2016).
[40] S. S. Dietrich and B. Berman, At. Data. Nucl. Data Tables **38**, 199 (1988).
[41] See Supplemental Material at http://link.aps.org/supplemental/10.1103/PhysRevC.99.052801 for the compilation of the properties of finite nuclei, nuclear matter, and neutron stars corresponding to the 28 representative EDFs as used in the present work along with the result obtained for the newly generated Skyrme forces SkΛ267 and SkΛ484; this material includes citations of Refs. [31,58–63].
[42] X.-H. Li, W.-J. Guo, B.-A. Li, L.-W. Chen, F. J. Fattoyev, and W. G. Newton, Phys. Lett. B **743**, 408 (2015).
[43] B.-A. Li, B.-J. Cai, L.-W. Chen, and J. Xu, Prog. Part. Nucl. Phys. **99**, 29 (2018).
[44] H.-Y. Kong, J. Xu, L.-W. Chen, B.-A. Li, and Y.-G. Ma, Phys. Rev. C **95**, 034324 (2017).
[45] B.-A. Li and X. Han, Phys. Lett. B **727**, 276 (2013).
[46] J. W. Holt, N. Kaiser, and G. A. Miller, Phys. Rev. C **93**, 064603 (2016).
[47] M. Baldo, L. M. Robledo, P. Schuck, and X. Viñas, Phys. Rev. C **95**, 014318 (2017).
[48] C. Mondal, B. K. Agrawal, J. N. De, S. K. Samaddar, M. Centelles, and X. Viñas, Phys. Rev. C **96**, 021302(R) (2017).
[49] B. K. Agrawal, S. K. Samaddar, J. N. De, C. Mondal, and S. De, Int. J. Mod. Phys. E **26**, 1750022 (2017).
[50] T. Malik, C. Mondal, B. K. Agrawal, J. N. De, and S. K. Samaddar, Phys. Rev. C **98**, 064316 (2018).
[51] J. Dobaczewski, W. Nazarewicz, and P.-G. Reinhard, J. Phys. G: Nucl. Part. Phys. **41**, 074001 (2014).
[52] C. Mondal, B. K. Agrawal, and J. N. De, Phys. Rev. C **92**, 024302 (2015).
[53] E. Chabanat, P. Bonche, P. Haensel, J. Meyer, and R. Schaeffer, Nucl. Phys. A **627**, 710 (1997).
[54] R. B. Wiringa, V. Fiks, and A. Fabrocini, Phys. Rev. C **38**, 1010 (1988).
[55] R. B. Wiringa, Rev. Mod. Phys. **65**, 231 (1993).
[56] T. Narikawa, N. Uchikata, K. Kawaguchi, K. Kiuchi, K. Kyutoku, M. Shibata, and H. Tagoshi, arXiv:1812.06100.
[57] Y. Fujimoto, K. Fukushima, and K. Murase, arXiv:1903.03400.
[58] C. Fuchs, Prog. Part. Nucl. Phys. **56**, 1 (2006).
[59] A. F. Fantina, N. Chamel, J. M. Pearson, and S. Goriely, EPJ Web Conf. **66**, 07005 (2014).
[60] P. Danielewicz, W. G. Lynch, and R. Lacey, Science **298**, 1592 (2002).
[61] K. Hebeler, J. M. Lattimer, C. J. Pethick, and A. Schwenk, Astrophys. J. **773**, 11 (2013).
[62] G. Colò, L. Cao, N. V. Giai, and L. Capelli, Comput. Phys. Commun. **184**, 142 (2013).
[63] M. Dutra, O. Lourenço, J. S. Sá Martins, A. Delfino, J. R. Stone, and P. D. Stevenson, Phys. Rev. C **85**, 035201 (2012).